The NASA Langley Laminar-Flow-Control Experiment on a Swept, Supercritical Airfoil

Suction Coefficient Analysis

Cuyler W. Brooks, Jr., Charles D. Harris, and William D. Harvey

NASA Technical Memorandum 4267

The NASA Langley Laminar-Flow-Control Experiment on a Swept, Supercritical Airfoil

Suction Coefficient Analysis

Cuyler W. Brooks, Jr., Charles D. Harris,
and William D. Harvey
Langley Research Center
*Hampton, Virginia*
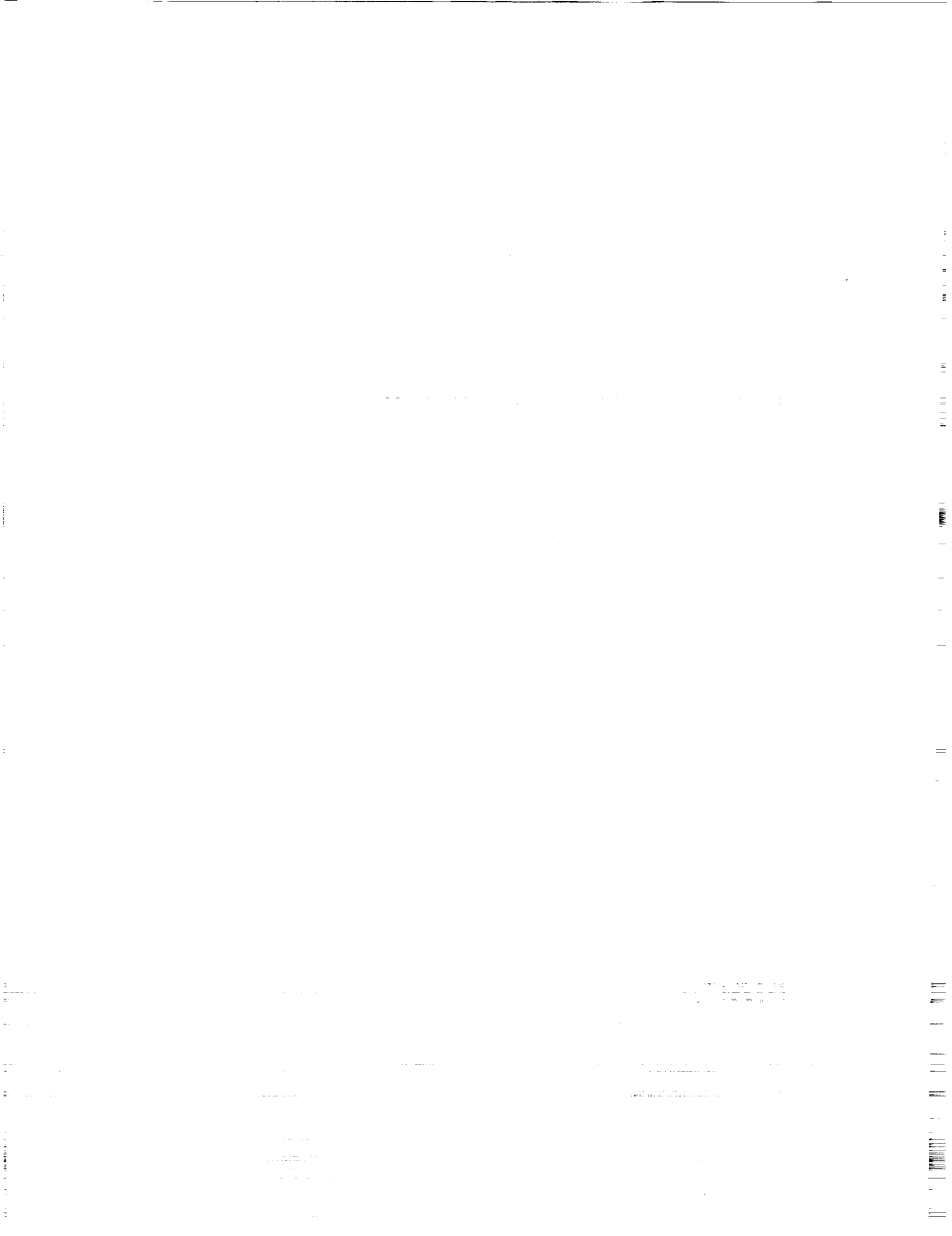
Summary

The Langley Research Center has designed and tested a swept, supercritical wing incorporating laminar flow control (LFC) at transonic flow conditions. Analytical expressions have been developed and an evaluation has been made of the experimental suction coefficient with the use of theoretical design information and experimental data.

The suction drag calculation is dependent on computation of the quantity of suction flow, represented as the suction coefficient. The definition of this coefficient and a derivation of the compressible and incompressible formulas for the computation of the coefficient from measurable quantities is presented in this paper.

The suction flow coefficient in the highest velocity nozzles is shown to be overpredicted by as much as 12 percent through the use of an incompressible formula. However, the overprediction in the computed value of suction drag due to using an incompressible computation of the flow coefficient when some of the suction nozzles were operating in the compressible flow regime is evaluated and found to be at most 6 percent at design conditions.

Introduction

The laminar-flow-control (LFC) experiments in the Langley 8-Foot Transonic Pressure Tunnel (8-ft TPT) on a swept, supercritical airfoil (ref. 1) investigated drag reduction through boundary-layer control by surface suction at transonic flow conditions. The quantity of suction at any point on the airfoil is represented by the suction coefficient, defined as the ratio of the mass flow normal to the suction surface to the mass flow in the free stream. The appropriate design value of this coefficient is determined from boundary-layer stability calculations for a particular airfoil and flow condition (refs. 2, 3, and 4). The computation of suction drag (ref. 5) from experimental data requires a value for this suction coefficient. The purpose of this paper is to present

(1) a derivation of the incompressible formula for the suction coefficient used in the 8-ft TPT experiment

(2) an analysis of the effect of the neglected compressibility terms on the accuracy of the computed suction drag coefficient.

Symbols

A area

b wing span, measured perpendicular to tunnel centerline

b_N wing span, measured along swept wing leading edge

$C_{p,N}$ local pressure coefficient, $\dfrac{p - p_\infty}{q_{\infty,N}}$

C_Q local suction coefficient, $\dfrac{-(\rho w)_{\text{ws}}}{(\rho U)_\infty}$

c wing chord, measured parallel to tunnel centerline

c_d section drag coefficient

$c_{l,N}$ normal section lift coefficient

c_N wing chord, measured perpendicular to wing leading edge

d_N diameter of nozzle

$E_{\text{sc},i}$ $= 0.2 M_\infty^2 + \dfrac{T_{t,\text{sc}}}{T_\infty} \left[\left(\dfrac{p_\infty}{p_{\text{sc}}} \right)^{\frac{\gamma-1}{\gamma}} - 1 \right]$

F area of duct in plane perpendicular to suction nozzle axis

f cross-sectional area of nozzle throat, $\dfrac{\pi d_N^2}{4}$

M Mach number

$\dot{m}$ mass flow

p pressure, psf

q dynamic pressure, psf

$q_{\infty,N}$ dynamic pressure based on normal leading-edge flow

R_c Reynolds number based on streamwise chord

s distance along surface

T temperature, °R

U velocity component in free-stream direction

u velocity component normal to leading edge, $U \cos \Lambda$

v velocity component parallel to leading edge, $U \sin \Lambda$

W velocity component perpendicular to free-stream direction and wing reference plane

w velocity component normal to surface

α_N nozzle-flow coefficient

γ	ratio of specific heats, 1.4 for air
Λ	wing sweep angle
ρ	density

See figures 1, 2, and 3 for geometric orientation of following coordinates:

X	coordinate in flow direction parallel to tunnel centerline
x	coordinate perpendicular to leading edge
Y	coordinate orthogonal to X in wing reference plane, positive up
y	coordinate parallel to leading edge, positive up
Z	coordinate orthogonal to X and Y
z	local surface normal, positive out from surface

Subscripts:

i	suction duct index
N	nozzle or normal
s	suction
sc	suction chamber
t	stagnation condition
ws	wing surface
∞	free stream

Abbreviations:

Comp.	compressible
Incomp.	incompressible
L.E.	leading edge
LFC	laminar flow control
T.E.	trailing edge
TPT	Transonic Pressure Tunnel

Experimental Apparatus and Model

A sketch of the LFC airfoil configuration, which incorporates laminar flow control into an advanced supercritical airfoil, and the shock-free design pressure distribution for this profile are shown in figure 1. Various types of boundary-layer instabilities taken into account during the design process are noted in the figure. This wing has a nearly full-chord discrete suction surface with an internal suction-flow ducting system. The continuous surface suction as modeled in the design theory can only be approached asymptotically by the actual suction surface of the

wind-tunnel model. For the LFC experiment in the 8-ft TPT (ref. 1), two suction surfaces were evaluated: one with narrow (about 0.003 inch) closely spaced spanwise slots and one with spanwise strips of perforated titanium approximately 0.5 inch wide and 0.4 inch apart (fig. 2(c)). Both suction concepts are discussed in more detail in references 1 (slotted) and 6 (perforated). Sketches of the design laminar flow test regions for these LFC wings are shown in figure 2.

The laminar flow regions are bounded by turbulent wedges that develop at the junctures of the tunnel liner wall and the wing. The upper-surface suction extends rearward to $X/c = 0.96$ on the central suction flap of the slotted wing and to $X/c = 0.89$ (the flap hinge line) on the porous-upper-surface wing. On the lower surface, only slotted suction was used and extends from $X/c = 0$ to 0.842. The model was mounted vertically in the wind tunnel and spanned the test section from ceiling to floor.

Figure 3 shows the geometric coordinate systems used in the suction flow analysis. Figure 4 shows the theoretical chordwise suction distributions at the minimum suction level required to maintain full-chord laminar flow over a range of Reynolds number for the upper and lower wing surfaces. The theoretical chordwise pressure distribution (fig. 1) was used as input to boundary-layer stability codes to determine these suction requirements. These results are derived from linear, parallel, incompressible boundary-layer stability analyses (refs. 2 and 4).

Analytical Methods

In order to analyze suction and wake drag, a swept LFC wing of constant cross section and infinite span in steady transonic flow is considered. The local suction velocity through the surface is assumed to be constant along lines parallel to the leading edge. The flow field over the wing is subdivided into a "suction flow" containing streamlines entering the wing suction surface, a "wake flow" containing streamlines entering the trailing-edge wake, and a "potential flow" containing all other streamlines. The suction system (fig. 2) consists of surface slots or perforations, internal airflow metering, ducting, and compressor. The suction flow passes through the suction system and is returned to the wind-tunnel circuit far enough downstream so as not to affect the wing wake.

The nondimensional suction coefficient is defined, in terms of a ratio of mass flow per unit area, as

$$C_Q = -\frac{(\rho w)_{\text{ws}}}{(\rho U)_\infty} \qquad (1)$$

where the negative sign indicates that the suction flow is *into* the wing surface.

The C_Q as defined by equation (1) is presented here because it is the way this coefficient is given in previous publications in the field. Nothing can be computed from equation (1) because $(\rho w)_{\text{ws}}$ is a local flow through an ideal porous wing with suction everywhere on the surface. On any physical wing, suction is discrete; that is, the suction flow passes through some discontinuous configuration of apertures in a solid nonporous wing surface material. The computable C_Q used in the LFC data reduction is derived as follows.

For each duct under the porous wing surface, continuity requires that the flow through the wing surface into the duct be equal to the flow extracted from the duct through the instrumented nozzle. In terms of the mass flow $\dot{m}$ for the porous wing surface of the ith duct,

$$\dot{m}_{\text{sc},i} = (\rho w)_{\text{ws}} A_{\text{ws}} = (\rho w)_{\text{sc},i} A_{\text{sc},i} \qquad (2)$$

where the area $A_{\text{sc},i} = (b_N \Delta c_N)_{\text{sc},i}$ is the part of the wing reference area assigned to the ith duct. Simplifying assumptions are made that this area, like the wing reference area, is a projected area on the wing chord plane and that the area $A_{\text{sc},i}$ includes such nonsuction regions as where the porous surface lies over bulkheads, in such a way that

$$\sum_{i=1}^{K} A_{\text{sc},i} = \sum_{i=1}^{K} (b_N \Delta c_N)_{\text{sc},i} = A_{\text{ref}} \qquad (3a)$$

and

$$\sum_{i=1}^{K} (\Delta c_N)_{\text{sc},i} = c_N \qquad (3b)$$

Note that both b_N (fig. 2(a)), the duct span parallel to the leading edge, and Δc_N (fig. 3), the duct chord segment perpendicular to the leading edge, vary with the duct index i.

The suction flow out of the duct is determined at the throat of the instrumented nozzle (see appendix of ref. 5) and thus is known to be

$$\dot{m}_{\text{sc},i} = \alpha_N \rho_N u_N f_{\text{sc},i} \qquad (4)$$

The suction mass flow for the ith duct $\dot{m}_{\text{sc},i}$ is now a measured quantity; thus, in equation (2), we can solve for the discrete mass flow per unit area (assumed constant over the porous face of the duct)

as follows:

$$(\rho w)_{\text{sc},i} = \frac{\dot{m}_{\text{sc},i}}{A_{\text{sc},i}} = \frac{\dot{m}_{\text{sc},i}}{(b_N \Delta c_N)_{\text{sc},i}} \qquad (5)$$

The suction coefficient used in the LFC data reduction is then defined as

$$(C_Q)_{\text{sc},i} = \frac{(\rho w)_{\text{sc},i}}{(\rho u)_\infty} = \frac{(\rho u)_{\text{sc},i}}{\rho_\infty u_\infty}$$
$$= \frac{\dot{m}_{\text{sc},i}}{\rho_\infty u_\infty (b_N \Delta c_N)_{\text{sc},i}} \qquad (6)$$

This is the quantity plotted in figure 4 as the discrete measured suction coefficient for comparison with the continuous theoretical suction coefficient. This $(C_Q)_{\text{sc},i}$ (referred to as "$C_{Q,\text{sc}}$" in ref. 5) is the quantity used to compute the suction drag coefficient using the equation derived in reference 5.

Equation (6) defines a local discrete suction coefficient where the computed mass flow through the porous face of each duct is nondimensionalized by the mass flow that would be seen for that duct if the porosity of the surface were 100 percent and the leading-edge-normal flow $(\rho_\infty u_\infty)$ were perpendicular to it. Because the $(b_N \Delta c_N)_{\text{sc},i}$ term is different for each duct, these $(C_Q)_{\text{sc},i}$ cannot be summed to compute a total C_Q. The use of this coefficient in equation (13) of reference 5 involves the summation of terms of the form

$$C_{Q,\text{sc}} E_{\text{sc}} d\left(\frac{s}{c}\right) = (C_Q)_{\text{sc},i} E_{\text{sc},i}(p,T) \frac{(\Delta c_N)_{\text{sc},i}}{c_N} \qquad (7)$$

where E is a function of the duct pressure and temperature. These terms are nondimensionalized on the same basis with respect to the wing chord because of the multiplication by $\frac{(\Delta c_N)_{\text{sc},i}}{c_N}$. With respect to the wing span the terms are nondimensionalized by the local duct span b_N over which the suction flow is assumed constant. Thus, these terms are proportional to mass flow per unit span, and the suction drag coefficient computed by the summation is thus a section drag coefficient, as indicated by the notation in reference 5.

In equation (6), $\dot{m}_{\text{sc},i}$ is the mass flow due to suction of the ith duct, which is located between successive chordwise stations s_i and s_{i+1} and has an average span b_N (fig. 2(a)) and chord Δc_N (measured parallel and perpendicular, respectively, to the leading edge), and the duct dimensions include one half the bulkhead wall thickness so that the sum of the duct areas is exactly equal to the wing surface area projected onto the chord plane.

Values of $(C_Q)_{sc,i}$ can be determined from flow quantity measurements of individual suction nozzles located in each duct (figs. 2(c) and 5). The derivation of a formula for the computation of $C_{Q,sc}$ from these measured quantities is based on specially designed and calibrated nozzles (as previously used by Pfenninger and Groth in low-drag suction airfoil flight and wind-tunnel tests (ref. 7)). Two expressions for the suction coefficient in terms of experimentally measured quantities are derived. The first expression (derived from the compressible Bernoulli equation) is accurate to the precision available from the instrumentation. The second, based on the incompressible Bernoulli equation, is the one used in the data reduction program throughout the LFC experiment in the 8-ft TPT; it is shown to give about 12 percent too high a value of the suction coefficient for the nozzles overdriven with higher than design throat velocity. At the flow velocities for which the nozzles were designed, up to 250 ft/sec, either expression yields very nearly the same result, but in the course of the LFC experiments, it was found necessary to increase the suction beyond the design value, which resulted in nozzle velocities greater than 500 ft/sec in some nozzles.

Compressible Solution

Figure 6 shows a schematic and photograph of typical LFC ducts and nozzles containing the suction flow. With the compressible Bernoulli equation (ref. 8) for either the duct or nozzle throat flow, one has the following equations:

in the nozzle throat,

$$\frac{1}{2}u_N^2 + \frac{\gamma}{\gamma-1}\frac{p_t}{\rho_t}\left(\frac{p_N}{p_t}\right)^{\frac{\gamma-1}{\gamma}} = \frac{\gamma}{\gamma-1}\frac{p_t}{\rho_t} \quad (8)$$

and in the duct,

$$\frac{1}{2}u_{sc}^2 + \frac{\gamma}{\gamma-1}\frac{p_t}{\rho_t}\left(\frac{p_{sc}}{p_t}\right)^{\frac{\gamma-1}{\gamma}} = \frac{\gamma}{\gamma-1}\frac{p_t}{\rho_t} \quad (9)$$

Solving these equations for p_N and p_{sc} and forming the difference $\Delta p = p_N - p_{sc} < 0$ give

$$\Delta p = p_t\left[\left(1 - \frac{u_N^2}{\frac{2\gamma}{\gamma-1}\frac{p_t}{\rho_t}}\right)^{\frac{\gamma}{\gamma-1}} - \left(1 - \frac{u_{sc}^2}{\frac{2\gamma}{\gamma-1}\frac{p_t}{\rho_t}}\right)^{\frac{\gamma}{\gamma-1}}\right] \quad (10)$$

Equation (10) can be considerably simplified with the observation that for $u_N < 600$ ft/sec and $u_{sc} < 200$ ft/sec, dropping the terms containing u_{sc} altogether results in a variation of only 2 psf in the value

of Δp. The pressure transducers used for the measurement of Δp had a precision at best of ± 1 psf. Therefore, in the inversion of equation (6) to solve for u_N as a function of the measured Δp, we can neglect the terms in u_{sc}, with the corresponding assumption (because $u_{sc} = 0$) that the stagnation values p_t and ρ_t can be replaced with the duct values p_{sc} and ρ_{sc}:

$$\Delta p = p_{sc}\left[1 - \frac{u_N^2}{\frac{2\gamma}{\gamma-1}\frac{p_{sc}}{\rho_{sc}}}\right]^{\frac{\gamma}{\gamma-1}} - 1 \quad (11)$$

It is now possible to solve explicitly for u_N:

$$u_N = \sqrt{\frac{2\gamma}{\gamma-1}\frac{p_{sc}}{\rho_{sc}}\left[1 - \left(\frac{\Delta p}{p_{sc}} + 1\right)^{\frac{\gamma-1}{\gamma}}\right]} \quad (12)$$

Using the isentropic compressible relation

$$\left(\frac{\rho_N}{\rho_{sc}}\right)^\gamma = \frac{p_N}{p_{sc}}$$

with $p_N = p_{sc} + \Delta p$, the throat density is

$$\rho_N = \rho_{sc}\left(\frac{p_{sc} + \Delta p}{p_{sc}}\right)^{1/\gamma} \quad (13)$$

Finally the mass flow at the nozzle throat for the ith duct is

$$\dot{m}_N = \alpha_N u_N \rho_N f \quad (14a)$$

where α_N is the nozzle flow efficiency coefficient for a given nozzle (discussed later) and f is the cross-sectional area of the nozzle throat. Substituting the expression for the mass flow into equation (6), the suction coefficient is then

$$(C_Q)_{sc,i} = \frac{(\alpha_N u_N \rho_N f)_i}{\rho_\infty u_\infty (b_N \Delta c_N)_{sc,i}}$$

or

$$(C_Q)_{sc,i} = \frac{\alpha_N f}{\rho_\infty U_\infty \cos\Lambda (b_N \Delta c_N)_{sc}}$$
$$\times \sqrt{\frac{2\gamma}{\gamma-1}\frac{p_{sc}}{\rho_{sc}}\left[1 - \left(\frac{\Delta p}{p_{sc}} + 1\right)^{\frac{\gamma-1}{\gamma}}\right]}$$
$$\times \rho_{sc}\left(\frac{p_{sc} + \Delta p}{p_{sc}}\right)^{1/\gamma} \quad (14b)$$

where $\rho_{sc} = \frac{p_{sc}}{RT_{sc}}$ and all the local variables must be evaluated for the ith duct.

4

Incompressible Solution

The formula actually used in the data reduction for the 8-ft TPT laminar-flow-control tests is derived as follows. The flow is taken to be incompressible, so that $\rho_N = \rho_{\text{sc}}$, and the incompressible Bernoulli equation then gives

$$p_N + \rho_N u_N^2 = p_{\text{sc}} + \rho_{\text{sc}} u_{\text{sc}}^2 \qquad (15)$$

Then the measured throat pressure drop is

$$\Delta p = p_N - p_{\text{sc}} = \frac{1}{2}\rho_N \left(u_{\text{sc}}^2 - u_N^2 \right) \qquad (16)$$

Dividing by the throat dynamic pressure, $q_N = \frac{1}{2}\rho_N u_N^2$, gives

$$\frac{\Delta p}{q_N} = \left(\frac{u_{\text{sc}}^2}{u_N^2} - 1 \right) \qquad (17)$$

But because we have assumed incompressible flow, the velocity must be inversely proportional to the area; therefore,

$$\frac{\Delta p}{q_N} = \frac{\Delta p}{\frac{1}{2}\rho_N u_N^2} = \left(\frac{f}{F} \right)^2 - 1 \qquad (18)$$

Solving for u_N, with $\rho_N = \rho_{\text{sc}}$ for incompressible flow, gives

$$u_N = \frac{\sqrt{\dfrac{-2\Delta p}{\rho_{\text{sc}}}}}{\sqrt{1 - (f/F)^2}} \qquad (19)$$

As for the compressible derivation, $\dot{m}_N = \alpha_N u_N \rho_{\text{sc}} f$, where α_N is the flow coefficient obtained by calibration. Therefore,

$$\dot{m}_N = \alpha_N f \frac{\sqrt{-2\Delta p \rho_{\text{sc}}}}{\sqrt{1 - (f/F)^2}} \qquad (20a)$$

and

$$(C_Q)_{\text{sc},i} = \frac{\alpha_N f \sqrt{\dfrac{\rho_{\text{sc}}}{\rho_\infty} \dfrac{\Delta p_N}{q_\infty}}}{(b_N \Delta c_N)_{\text{sc},i} \cos \Lambda \sqrt{1 - (f/F)^2}} \qquad (20b)$$

where $\Delta p_N = p_{\text{sc}} - p_N = -\Delta p > 0$ is a required measurement. The $\cos \Lambda$ in the denominator is required because $C_{Q,\text{sc}}$ is defined in equation (2) as nondimensionalized by $u_\infty = U_\infty \cos \Lambda$, but the q_∞ that is most convenient to use in equation (20b) is the free-stream dynamic pressure $q_\infty = \frac{1}{2}\rho_\infty U_\infty^2$.

Comparison of Solutions

Note that equation (14b), which includes compressibility effects, and equation (20b), which does not, give $C_{Q,\text{sc}}$ as a function of the same variables, except that equation (14b) does not use the suction duct area F.

The difference in these two solutions for $(C_Q)_{\text{sc},i}$ as a function of nozzle throat venturi pressure Δp_N is shown in figure 7, along with the exact compressible Bernoulli equation solution for Δp_N as a function of $(C_Q)_{\text{sc},i}$. It can be seen that for the lower values of Δp_N, the curves are almost coincident, but as Δp_N and $(C_Q)_{\text{sc},i}$ increase, the incompressible solution (eq. (20b)) increasingly overpredicts $(C_Q)_{\text{sc},i}$ at a given Δp_N, whereas the compressible solution (eq. (14b)), even with the approximations made to permit an explicit expression for $(C_Q)_{\text{sc},i}$, yields essentially the same result as the exact compressible Bernoulli equation. In reference 1, the design limit for velocity in the calibrated nozzles is given as 250 ft/sec. Up to this velocity, the compressibility effects are negligible and equation (20b) agrees with equation (14b) and the exact compressible solution. In the actual test, however, a number of nozzles were pushed to almost 600 ft/sec, resulting in up to a 12-percent overprediction of $\dot{m}$ by the incompressible solution. This compressibility effect on the computed mass flow in the overdriven nozzles was not evaluated until after the test was over and thus was not included in the data reduction computer program until after very large quantities of reduced data had been produced.

Calibrated Nozzle and Nozzle-Flow Coefficient α_N

A sketch of the three-dimensional suction nozzle previously used by Pfenninger and Groth (ref. 7) and considered herein is shown in figure 5. The nozzle-flow coefficient α_N is a function of Reynolds number (based on nozzle diameter) as determined by calibration. An empirical equation for the diameter of the nozzle from the beginning of the contraction to the throat is

$$d(x) = d_N \left(1 + \frac{3}{2} \left\{ \frac{4}{\pi} \arctan \left[1 - \left(\frac{x}{2d_N} \right)^n \right] \right\}^{1/n} \right)$$

$$(0 \leq x \leq 2d_N) \quad (21)$$

where d_N is the nozzle throat diameter and the exponent $n = 2.545$.

This equation fits the nozzle coordinates from the entrance plane ($x = 0$) to the throat where

p_N is measured ($x = 2d_N$) to within 0.01 inch for $d_N = 1$ inch. In the 8-ft TPT LFC experiments, twelve sizes of this nozzle were used, with $d_N = 0.188$ to 0.875 inch.

The data reduction procedure obtains the value of α_N from an empirical equation fitted to the nozzle calibration data. The fit of the empirical equation to the data is within the error band of the calibration data. The empirical equation used in the LFC data reduction is

$$
\alpha_N(R_d) = 0.927
$$
$$
- 0.0339787 \left[\sqrt{1 + 4(\log_{10} R_d - 4)^2} - 1 \right]
$$
$$
+ 0.075(\log_{10} R_d - 4) \tag{22}
$$

where R_d is the Reynolds number of the nozzle throat flow based on the nozzle throat diameter, d_N. Equations (21) and (22) were fitted to unpublished data provided by Werner Pfenninger in the range $10^3 < R_d < 10^5$.

Evaluation of Suction Drag Coefficient

Inspection of equation (20b) for the suction mass-flow coefficient reveals that $C_{Q,\text{sc}}$ is proportional to $\sqrt{\Delta p_N}$ with all other quantities constant, except for the effect of α_N, which is a function of nozzle throat Reynolds number and is determined from calibration. Therefore, low-drag experiments involving determination of the suction drag as part of the total drag should, when applying equation (20b) or (14b), analyze the data accuracy required and select a suitable measurement technique (instrumentation).

The suction drag expressed in integral form as equation (13) of reference 5 is

$$
c_{d,s} = \frac{\cos \Lambda}{0.2 M_\infty^2} \int_{\text{L.E.}}^{\text{T.E.}} C_{Q,\text{sc}}
$$
$$
\times \left\{ 0.2 M_\infty^2 + \frac{T_{t,\text{sc}}}{T_\infty} \left[\left(\frac{p_\infty}{p_{\text{sc}}} \right)^{\frac{\gamma-1}{\gamma}} - 1 \right] \right\} d\left(\frac{s}{c} \right)
$$
$$
\tag{23a}
$$

and is discretized for computation as

$$
c_{d,s} = \sum_{i=1}^{K} (C_Q)_{\text{sc},i} E_{\text{sc},i}(T_{\text{sc}}, p_{\text{sc}}) \frac{(\Delta c_N)_{\text{sc},i}}{c_N} \tag{23b}
$$

Sample Computation

As an example of the use of equations (20b) and (23b) in the data reduction process, the terms of the equation are computed for duct 9 (a typical duct in the center of the upper surface) for a typical case at design Reynolds number ($R_c = 20 \times 10^6$) for the slotted LFC experiment. Taking the terms in order from left to right,

$$
\Lambda = 23°
$$
$$
M_\infty = 0.8188
$$
$$
T_{t,\infty} = 547.54°\text{R}
$$
$$
p_\infty = 937.3 \text{ psf}
$$

and thus (from the standard adiabatic perfect gas equation for M_∞ and $T_{t,\infty}$), $T_\infty = 482.80°\text{R}$.

For measured values of the nozzle throat pressure drop $\Delta p_N = 29.28$ psf, duct temperature $T_{t,\text{sc}} = 532.17°\text{R}$, and duct static pressure $p_{\text{sc}} = 433.98$ psf, $(C_Q)_{\text{sc},i}$ for duct 9 may be calculated from equation (20b) to be

$$
(C_Q)_{\text{sc},9} = 0.000122285
$$

and the contribution of this duct to the suction drag coefficient is

$$
(\Delta c_d)_{\text{sc},9} = 0.00002555
$$

Alternatively, $C_{Q,\text{sc}}$ may be computed from the more exact compressible equation (14b) to obtain

$$
(C_Q)_{\text{sc},9} = 0.0001189
$$
$$
(\Delta c_d)_{\text{sc},9} = 0.00002486
$$

It should be noted that the numbers in this example are given to greater precision than is actually available from the instrumentation. In general, pressure errors are at least on the order of 1 psf (except for the instruments used to measure tunnel total and static pressures, which are accurate to 0.2 psf, giving a Mach number precision of 0.0007) and temperature errors at least $\pm 1°\text{R}$. Based on these estimates, the number computed as the $(C_Q)_{\text{sc},9}$ of duct 9 (0.000122285) has a possible error of ± 0.000002 ($C_{Q,\text{sc}} = 0.000120$ to 0.000124), and the computed suction drag coefficient has a possible error of ± 0.000001 (Duct 9 $(\Delta c_d)_{\text{sc},9} = 0.000024$ to 0.000026). Thus, the systematic error in $c_{d,s}$ due to use of the incompressible equation (20b) is less than that caused by the random uncertainty of 1 psf in the pressure measurement at the nozzle throat (as long as only a few nozzles at any given time have excessive velocities, which was the case in these tests).

Figure 7 shows the comparison of the exact compressible Bernoulli equation, the approximation

based on neglecting u_{sc} (eq. (14b)), and the incompressible approximation (eq. (20b)), with a typical high velocity nozzle data point indicated on the curve. The nozzle throat Mach number M_N is also presented in this figure. It can be seen that for $M_N < 0.3$, all three methods give the same result, but for $M_N > 0.3$, the incompressible method is increasingly in error, while the approximate compressible (eq. (14b)) solution remains essentially equivalent to the complete compressible Bernoulli equation (which cannot be made explicit for $\dot{m}$ as a function of Δp).

The experimental accuracy to which the suction drag coefficient can be determined for a single duct is primarily dependent upon the accuracy to which Δp (the drop in pressure from the duct to the nozzle throat) can be measured. The use of the incompressible approximation yields values of flow coefficient that are up to 12 percent too high for the nozzles with highest flow velocity. This results in a corresponding error in the suction drag contribution from those nozzles. However, since only a few nozzles have such high velocities, the cumulative error in the overall suction drag due to the incompressible approximation is small. Recomputation of sample cases at design conditions (table I) shows that the upper-surface laminar region has a compressible-method (eq. (14b)) suction drag coefficient 4 to 6 percent lower than the corresponding incompressible (eq. (20b)) value. The major error still lies in the fact that the basic measurement of Δp, which varies from -15 to -130 psf over the wing at design conditions, had to be made with instrumentation having an error estimated at ± 1 psf.

Concluding Remarks

The Langley Research Center has designed and tested a swept, supercritical wing incorporating laminar flow control (LFC) at transonic flow conditions. Analytical expressions have been developed and an evaluation has been made of the experimental suction coefficient with the use of theoretical design information and experimental data.

The suction drag calculation is dependent on computation of the quantity of suction flow, represented as the suction coefficient. The definition of this coefficient and a derivation of the compressible and incompressible formulas for the computation of the coefficient from measurable quantities is presented in this paper.

The suction flow coefficient in the highest velocity nozzles is shown to be overpredicted by as much as 12 percent through the use of an incompressible formula. However, the overprediction in the computed value of suction drag due to using an incompressible computation of the flow coefficient when some of the suction nozzles were operating in the compressible flow regime is evaluated and found to be at most 6 percent at design conditions.

References

1. Harris, Charles D.; Harvey, William D.; and Brooks, Cuyler W., Jr.: *The NASA Langley Laminar-Flow-Control Experiment on a Swept, Supercritical Airfoil—Design Overview.* NASA TP-2809, 1988.

2. Dagenhart, J. Ray: *Amplified Crossflow Disturbances in the Laminar Boundary Layer on Swept Wings With Suction.* NASA TP-1902, 1981.

3. El-Hady, Nabil M.: On the Stability of Three-Dimensional Compressible Nonparallel Boundary Layers. AIAA-80-1374, July 1980.

4. Mack, Leslie M.: On the Stability of the Boundary Layer on a Transonic Swept Wing. AIAA-79-0264, Jan. 1979.

5. Brooks, Cuyler W., Jr.; Harris, Charles D.; and Harvey, William D.: *The NASA Langley Laminar-Flow-Control Experiment on a Swept, Supercritical Airfoil—Drag Equations.* NASA TM-4096, 1989.

6. Maddalon, Dal V.; and Poppen, William A., Jr.: *Design and Fabrication of Large Suction Panels With Perforated Surfaces for Laminar Flow Control Testing in a Transonic Wind Tunnel.* NASA TM-89011, 1986.

7. Pfenninger, W.; and Groth, E.: Low Drag Boundary Layer Suction Experiments in Flight on a Wing Glove of an F-94A Airplane With Suction Through a Large Number of Fine Slots. *Boundary Layer and Flow Control,* Volume 2, G. V. Lachmann, ed., Pergamon Press, 1961, pp. 981–999.

8. Liepmann, H. W.; and Roshko, A.: *Elements of Gasdynamics.* John Wiley & Sons, Inc., c.1957.
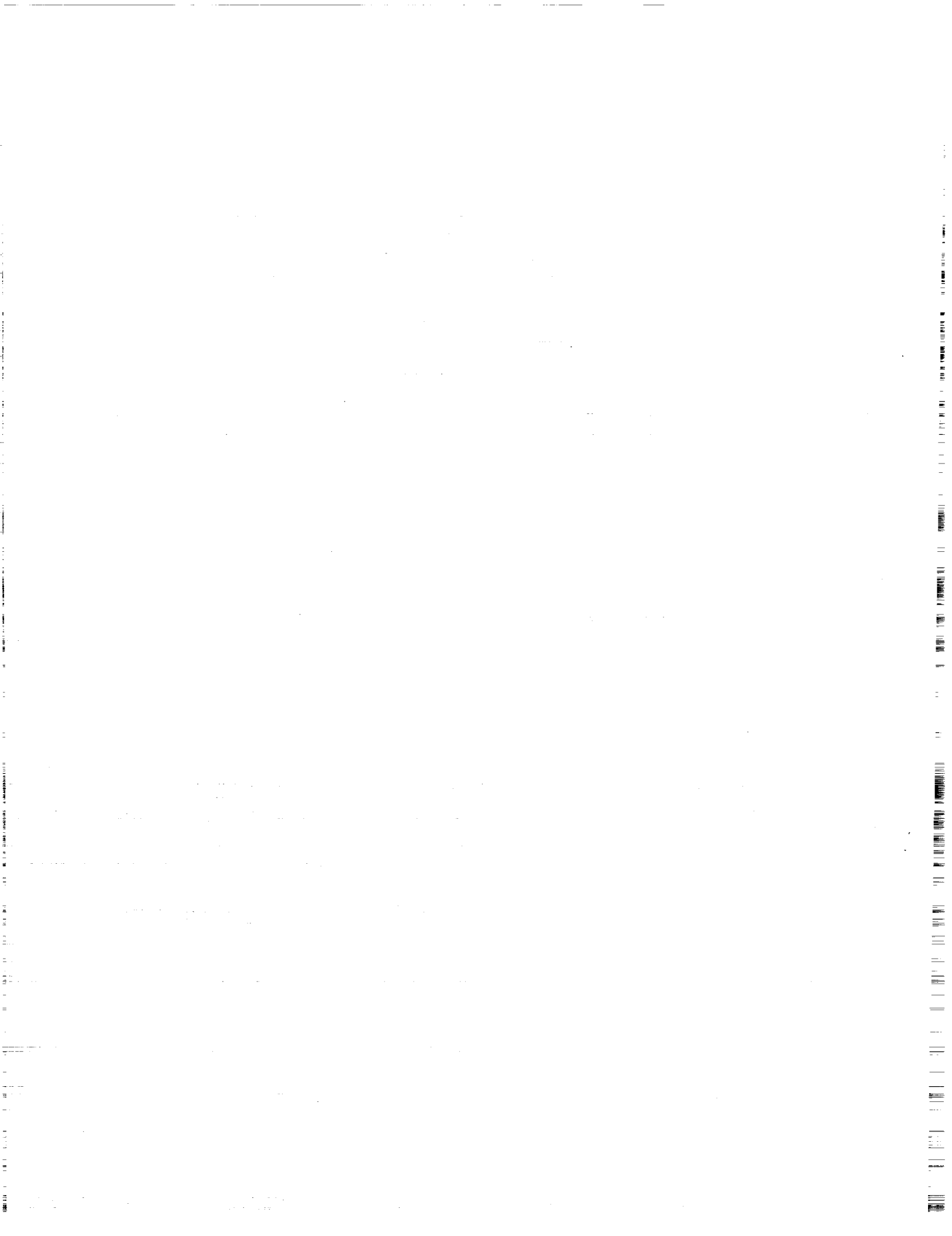
Table I. Effect of Compressibility Correction on
Typical LFC Suction Drag Data

Airfoil	R_c	Suction level	Maximum velocity in nozzle throat (laminar region), ft/sec		Suction drag, $c_{d,sc}$		Change, percent
			Incomp.	Comp.	Incomp.	Comp.	
Porous upper surface	20×10^6	High	495	507	0.00164	0.00156	−5
	20	Low	406	411	.00119	.00114	−4
	10	High	501	515	.00163	.00154	−6
Slotted upper surface	10×10^6	High	546	560	0.00231	0.00217	−6
	10	Low	464	473	.00160	.00153	−4
	20	High	565	582	.00244	.00229	−6
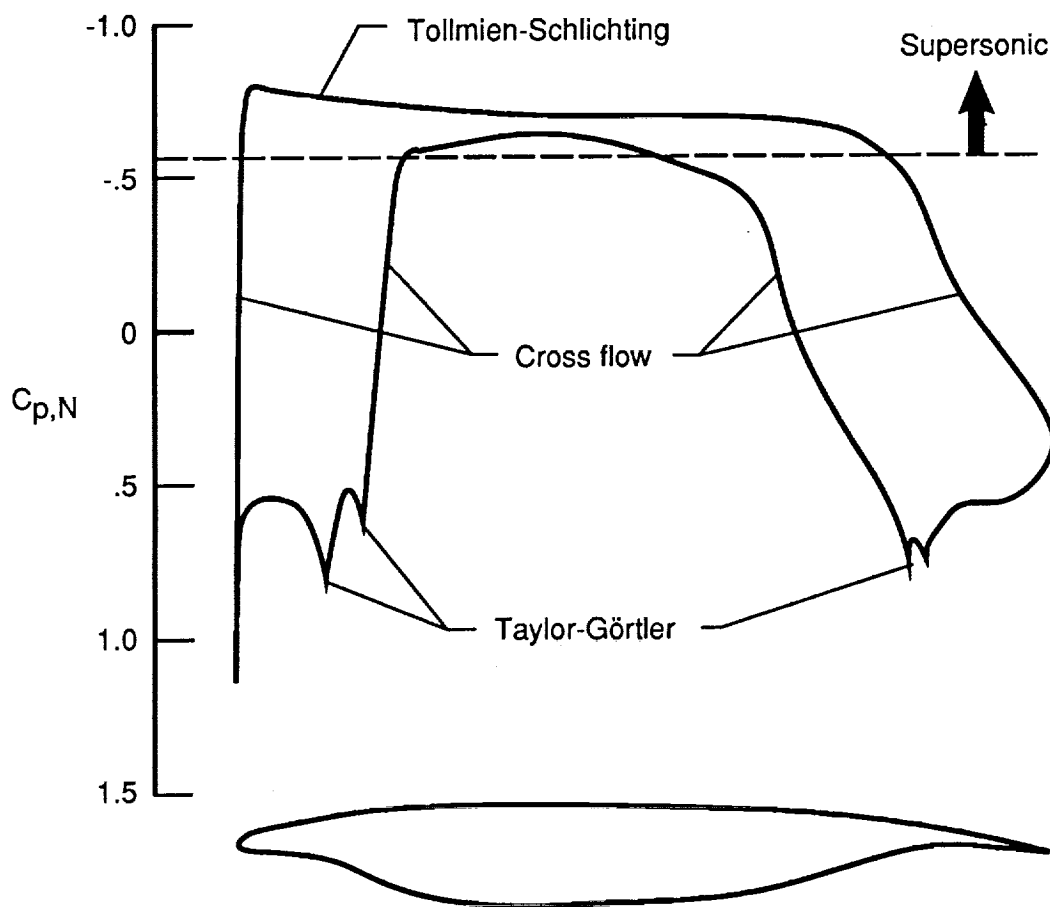
Figure 1. Airfoil geometry and pressure distribution (computed by two-dimensional compressible theory with $M = M_\infty \cos \Lambda = 0.755$) with indicated boundary-layer instability regions on swept, supercritical LFC airfoil. $c_{l,N} = 0.55$; $M_\infty = 0.82$; $\Lambda = 23°$.
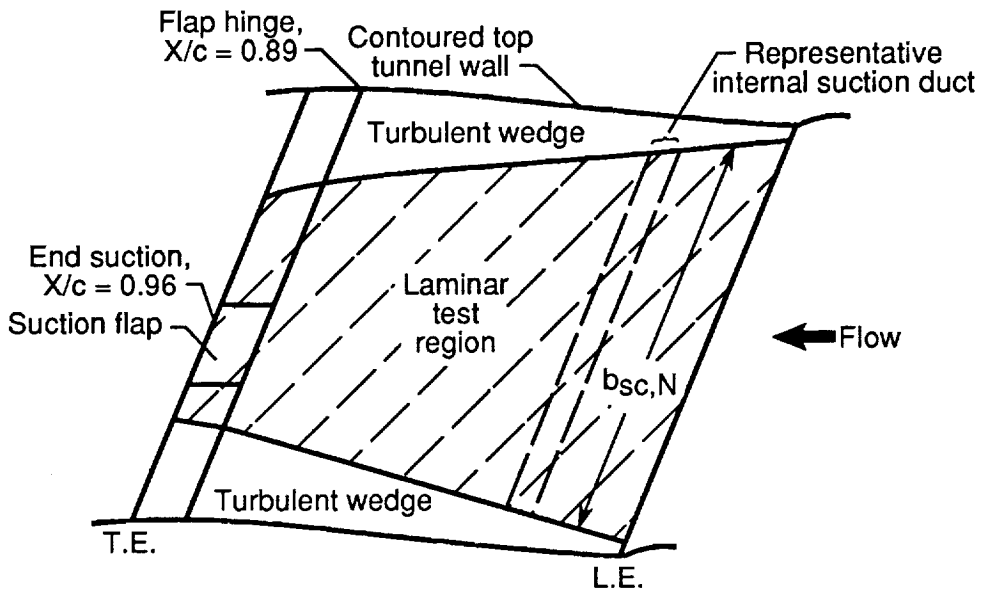
(a) Upper-surface test region.
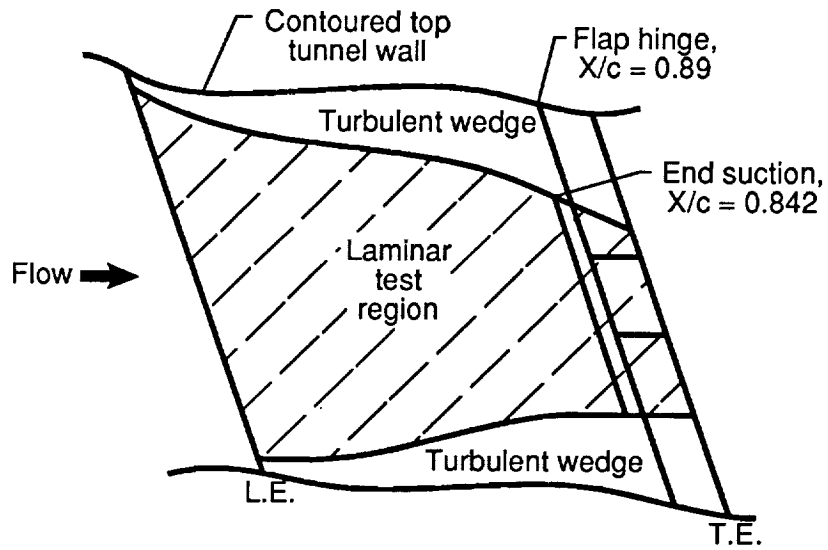
(b) Lower-surface test region.

Figure 2. Sketch of LFC airfoil laminar test region with suction (hatched region).

11

Slotted skin-plenum-duct design

Porous skin-flute-duct design
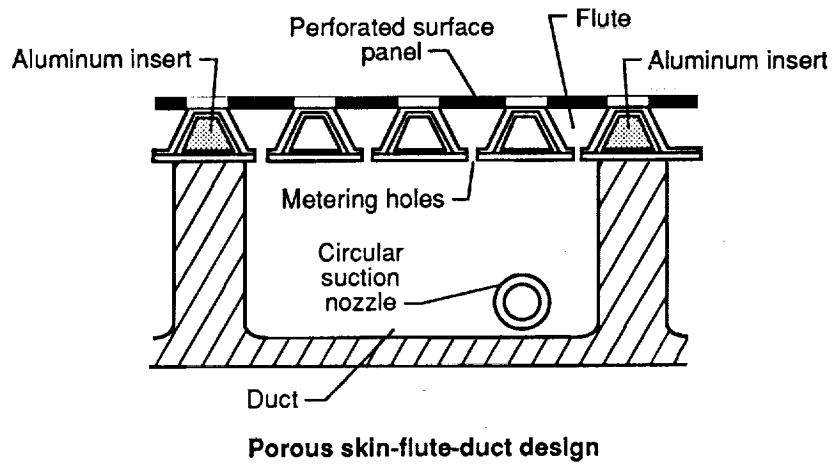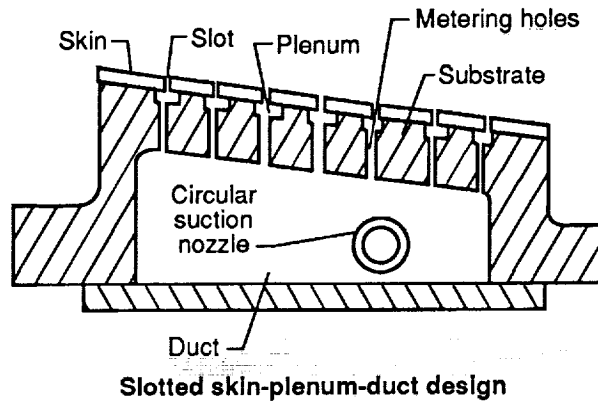
(c) Suction system design cross sections.

Figure 2. Concluded.
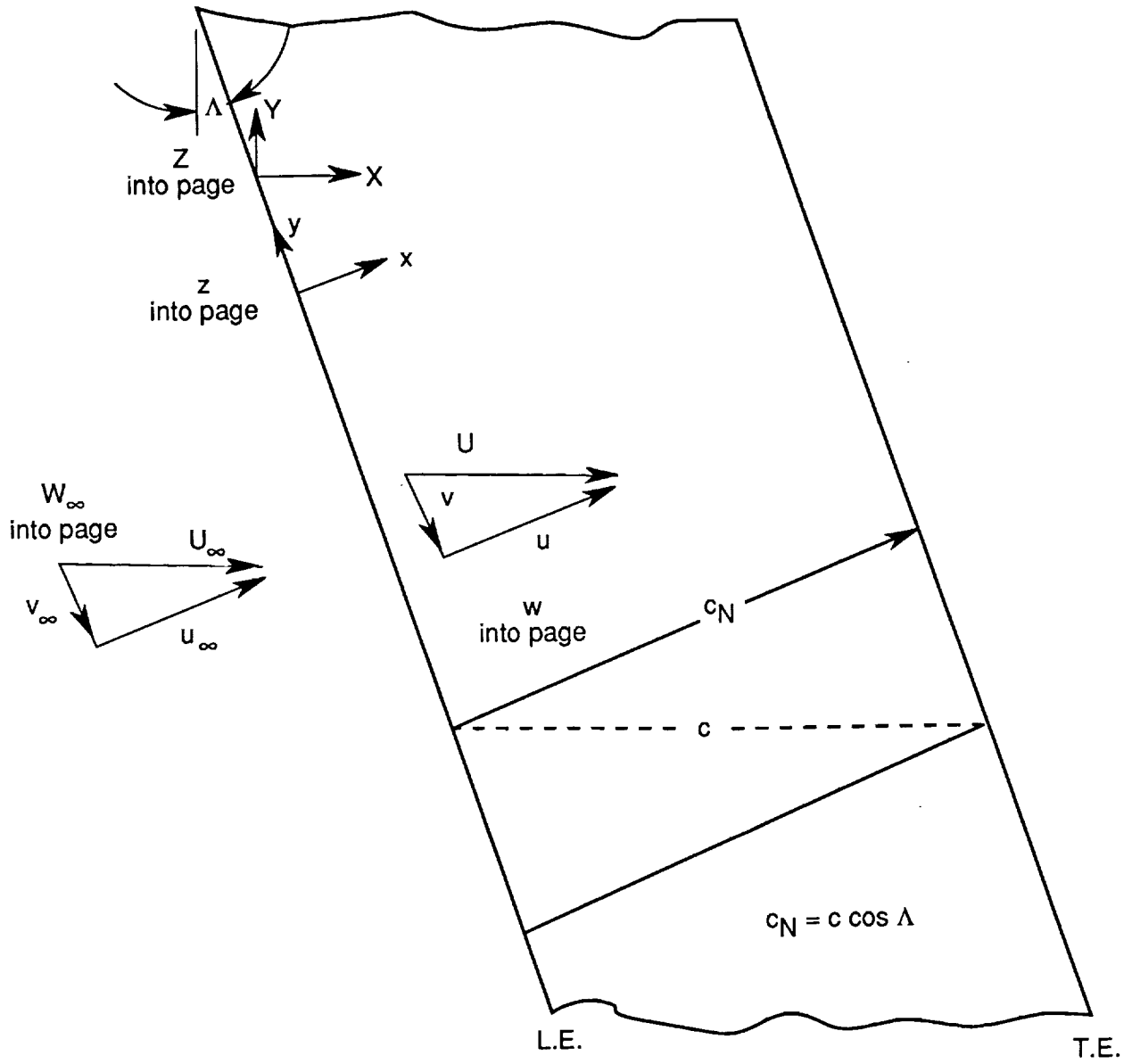
Figure 3. Flow analysis coordinate systems.
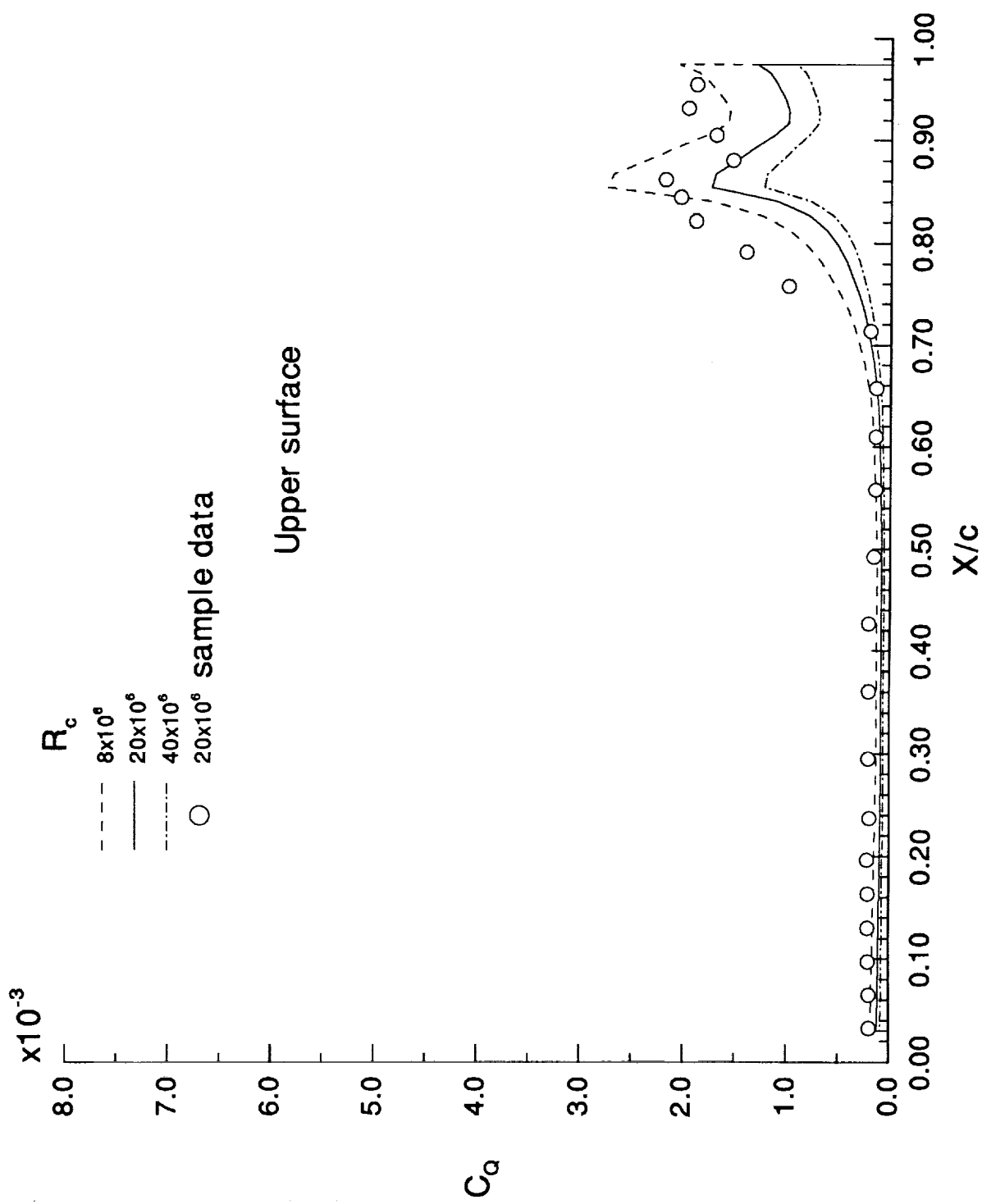
Figure 4. Theoretical variation of suction coefficient along chord for full chord laminar flow over LFC airfoil at design condition. $c_{l,N} = 0.55$; $M_\infty = 0.82$; $\Lambda = 23°$.
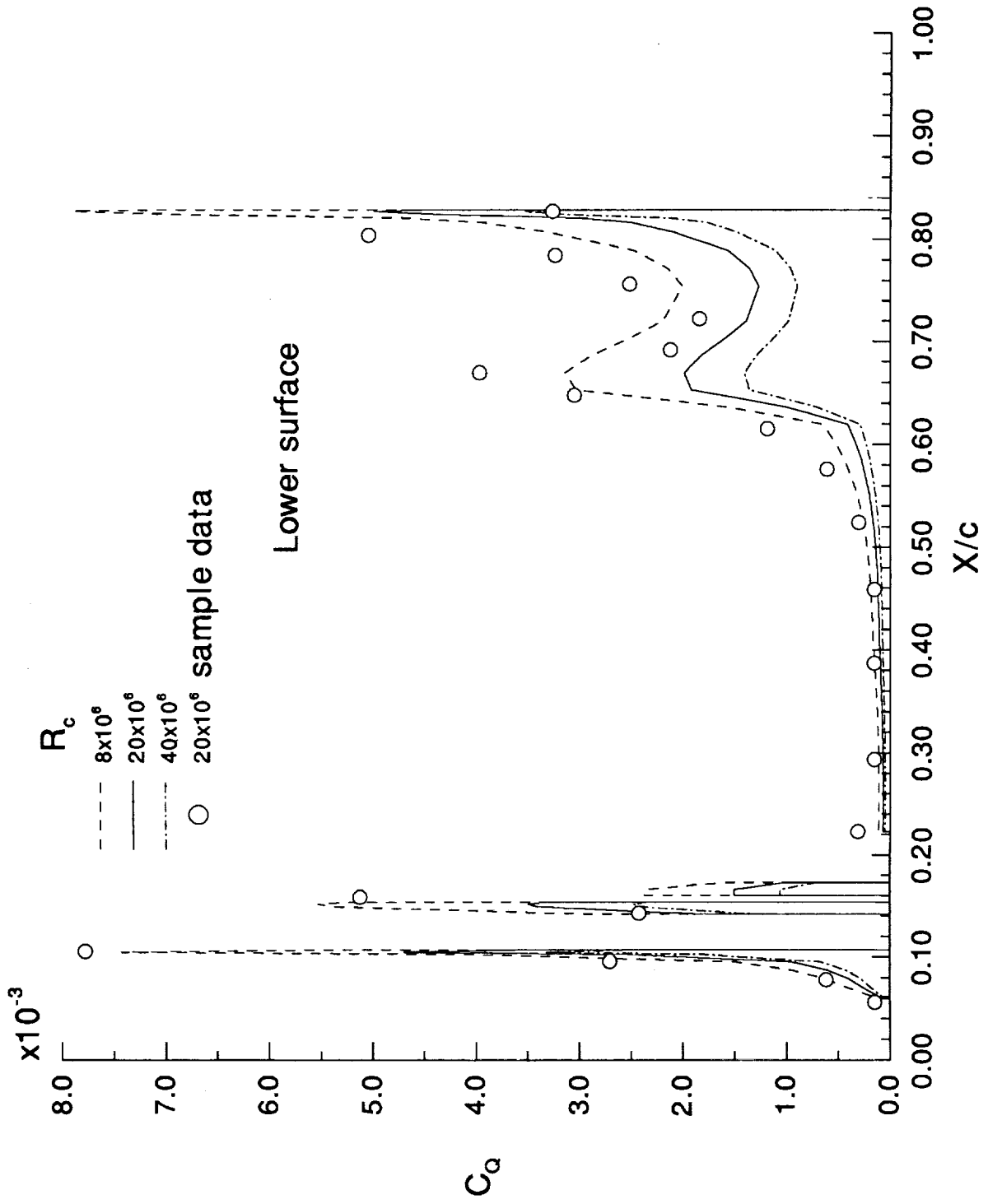
Figure 4. Concluded.
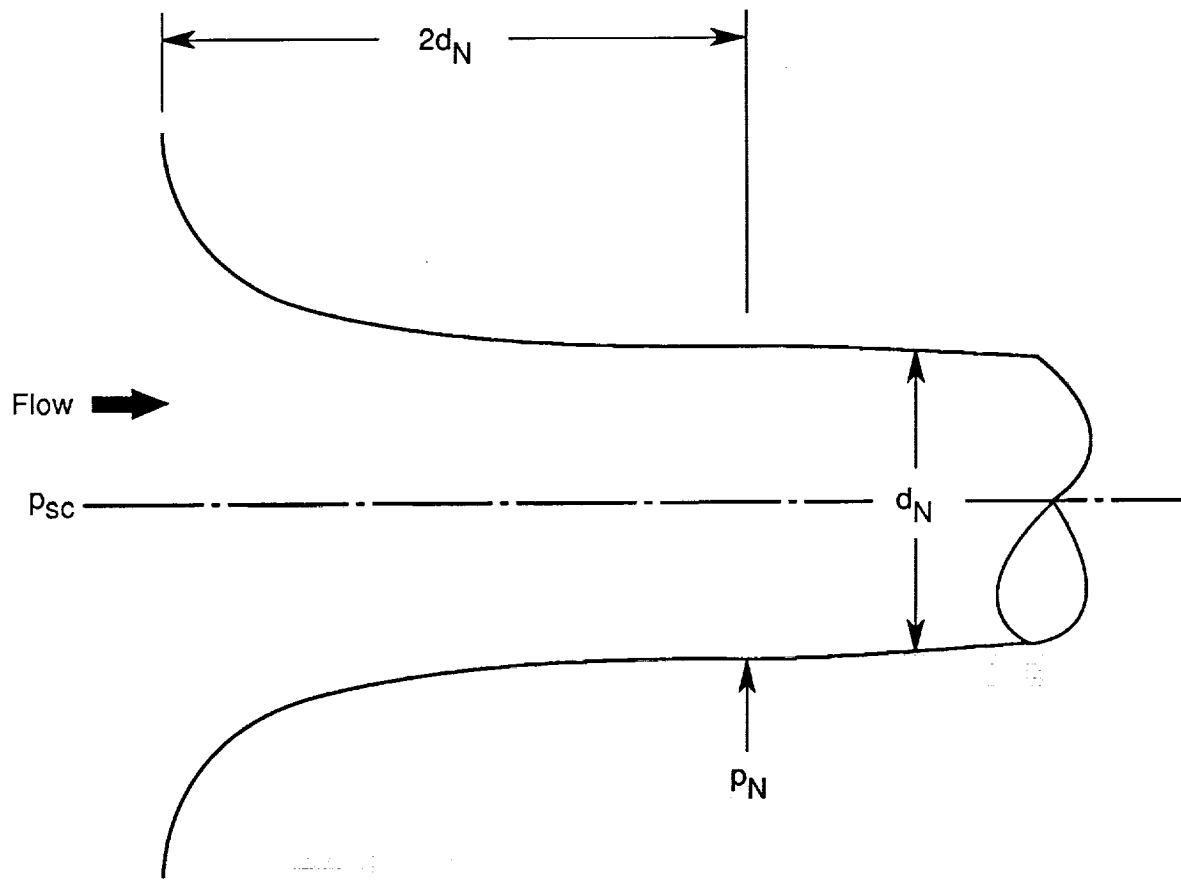
Figure 5. Sketch of calibrated suction nozzle.

Exterior flow

← Slotted or porous surface

← Metering hole surface

Duct

Duct static pressure, p_{SC}

Nozzle throat
pressure, p_N
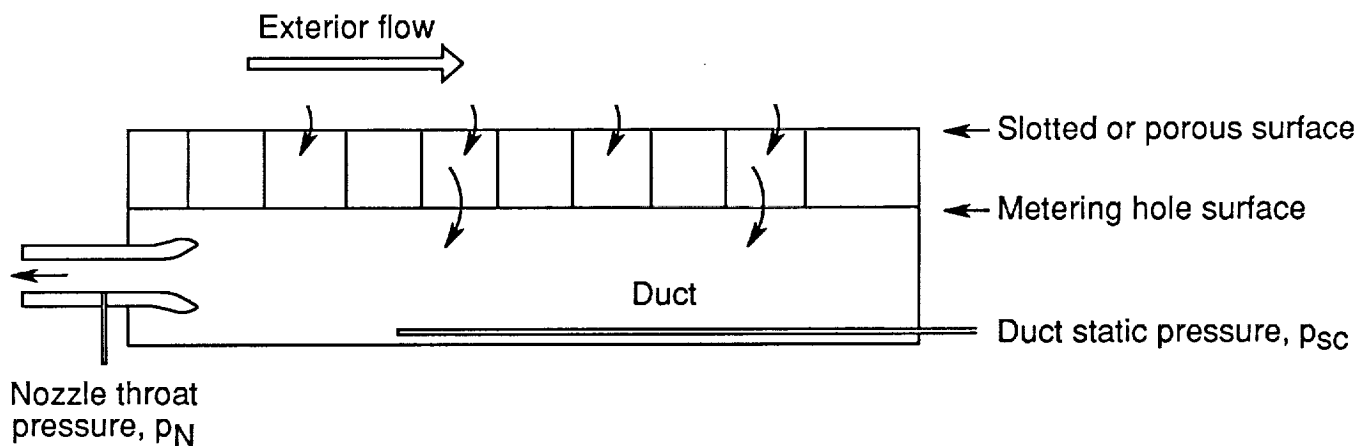
(a) Schematic of LFC suction flow passages.
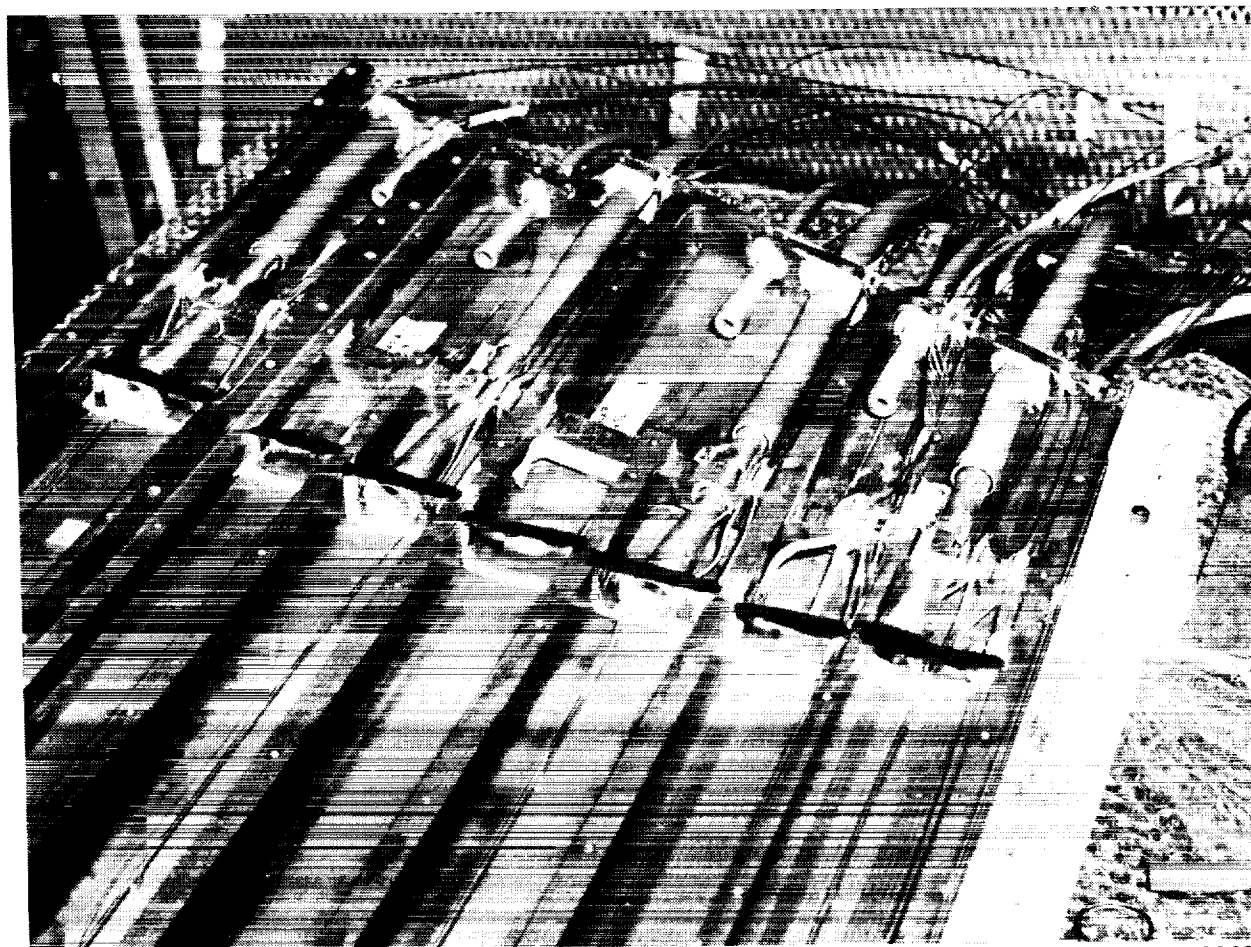
L-81-8068

(b) Typical LFC suction ducts and nozzles.

Figure 6. Suction system.
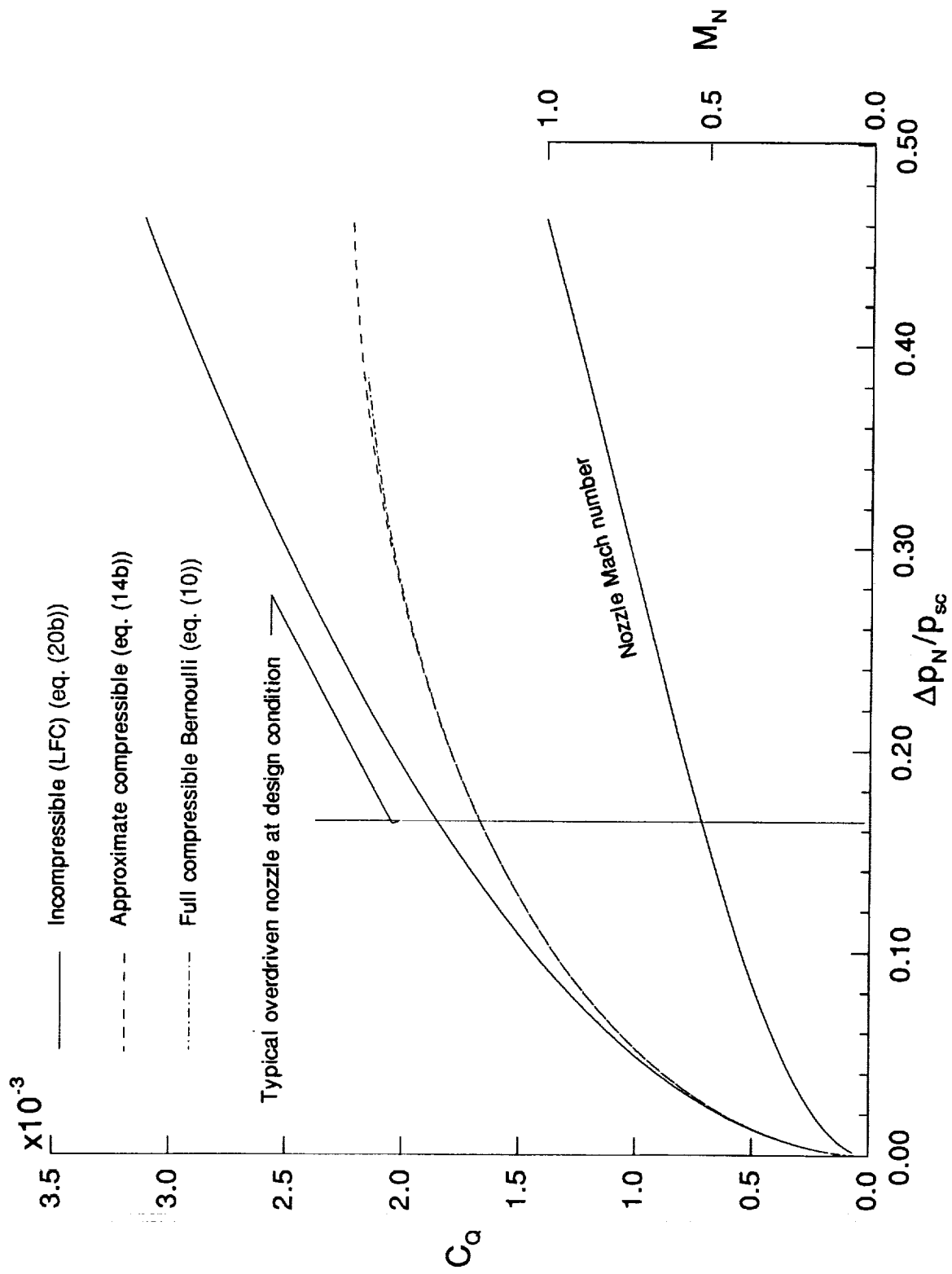
Figure 7. Variation of suction coefficient and nozzle throat Mach number with nozzle venturi pressure drop for typical LFC nozzle.

NASA National Aeronautics and Space Administration	Report Documentation Page	
1. Report No. NASA TM-4267	2. Government Accession No.	3. Recipient's Catalog No.
4. Title and Subtitle The NASA Langley Laminar-Flow-Control Experiment on a Swept, Supercritical Airfoil *Suction Coefficient Analysis*		5. Report Date June 1991
		6. Performing Organization Code
7. Author(s) Cuyler W. Brooks, Jr., Charles D. Harris, and William D. Harvey		8. Performing Organization Report No. L-16774
		10. Work Unit No. 505-61-21-03
9. Performing Organization Name and Address NASA Langley Research Center Hampton, VA 23665-5225		
		11. Contract or Grant No.
12. Sponsoring Agency Name and Address National Aeronautics and Space Administration Washington, DC 20546-0001		13. Type of Report and Period Covered Technical Memorandum
		14. Sponsoring Agency Code

15. Supplementary Notes

16. Abstract

The Langley Research Center has designed and tested a swept, supercritical airfoil incorporating laminar flow control (LFC) at transonic flow conditions. The definition of an experimental suction coefficient and a derivation of the compressible and incompressible formulas for the computation of the coefficient from measurable quantities is presented in this paper. The suction flow coefficient in the highest velocity nozzles is shown to be overpredicted by as much as 12 percent through the use of an incompressible formula. However, the overprediction in the computed value of suction drag when some of the suction nozzles were operating in the compressible flow regime is evaluated and found to be at most 6 percent at design conditions.

17. Key Words (Suggested by Author(s)) Laminar-flow control Swept, supercritical airfoil Suction	18. Distribution Statement Unclassified—Unlimited Subject Category 02		
19. Security Classif. (of this report) Unclassified	20. Security Classif. (of this page) Unclassified	21. No. of Pages 19	22. Price A02